Evolution of the Structure and Magnetic Properties of FeCo Nanoparticles in an Alumina Aerogel Matrix

Anna Corrias,* Maria F. Casula, Andrea Falqui, and Giorgio Paschina

Dipartimento di Scienze Chimiche, Università di Cagliari, Complesso Universitario, S.S. 554 bivio per Sestu, 09042 Monserrato, Cagliari, Italy

Received February 9, 2004. Revised Manuscript Received May 27, 2004

Nanocrystalline γ-Al_2O_3 and FeCo−Al_2O_3 nanocomposite aerogels with high surface areas and pore volumes were prepared by high-temperature supercritical drying of alcogels obtained by a fast sol−gel procedure. The formation of γ-Al_2O_3 occurs via a sequence of stages: in the parent aerogel an alkyl derivative of boehmite is observed whose calcination gives rise to a disordered phase and finally to γ-Al_2O_3 which is stable up to 1000 °C. In the presence of iron and cobalt, calcination of the aerogel gives rise to a spinel phase similar to γ-Al_2O_3 where metal ions partially fill the vacancies. Nanocomposites constituted of FeCo alloy nanoparticles dispersed into γ-Al_2O_3 matrix are obtained via reduction in hydrogen flow of the aerogels containing iron and cobalt. The amount and average size of the nanoparticles depends both on the temperature and time of the reduction treatment and affects the resulting magnetic properties. All the reduced aerogels show superparamagnetic behavior, but the collective magnetic properties are strongly dependent on the amount and mean size of the alloy nanoparticles.

1. Introduction

Aerogels are materials with unique properties which stem from their highly extended and open porosity, very low densities, and high inner surface areas.[1,2] They are prepared by the sol−gel process through special drying techniques which avoid the capillary forces at the liquid/vapor interface responsible for shrinkage and cracking, therefore preserving the original porous structure of the alcogels.[3]

The majority of the studies in this field has been devoted to single-metal oxide aerogels, and in particular the most investigated system is by far SiO_2. Multicomponent oxide aerogels can also be obtained by co-gelation of different metal precursors; in this case the preparation can lead either to homogeneous mixed metal oxide aerogels or to heterogeneous products, depending on the precursor reactivity. When heterogeneous aerogels are obtained, they are frequently nanocomposite materials; that is, one metal oxide is present as a nanocrystalline phase dispersed into the other phase which acts as a matrix.[4−6] Such nanocomposites are of great interest because they combine individual properties of the constituent phases, giving rise to new functional materials.[7,8]

By conversion of the metal oxides through treatment with a reducing gas flow, the dispersed phase can be easily obtained as a metal phase. The preparation of such composites is favored in aerogel materials as a consequence of their high surface area and pore volume, which improve the effectiveness of the reducing treatment.

Recently, FeCo−SiO_2 nanocomposites constituted of FeCo alloy nanoparticles dispersed into amorphous silica were obtained in the form of xerogel, aerogel, and films.[9−11] These materials, which were obtained by co-gelation of Si alcoxide and either Co and Fe nitrates or acetates, are of interest since FeCo alloys have attractive size-dependent magnetic properties which can be strongly affected by interparticle interactions;[12] moreover, FeCo-supported particles can be exploited for catalytic applications.[13] The aerogel samples showed to be very easily reducible, giving rise to FeCo nanocrystalline particles with the desired composition; on the other hand, unalloyed cobalt and metal oxide are frequently obtained together with the FeCo alloy in xerogel samples.[14] The different results are ascribed to

* To whom correspondence should be addressed. Tel: +39 070 6754351. Fax: +39 070 6754388. E-mail: corrias@unica.it.

(1) Hüsing, N.; Schubert, U. *Angew. Chem., Int. Ed.* **1998**, *37*, 22.
(2) Pierre, A. C.; Pajonk, G. M. *Chem. Rev.* **2002**, *102*, 4243.
(3) Brinker, C. J.; Scherer, G. W. *Sol−Gel Science*; Academic Press: San Diego, 1990.
(4) Casula, M. F.; Corrias, A.; Paschina, G. *J. Mater. Res.* **2000**, *15*, 2187.
(5) Casula, M. F.; Corrias, A.; Paschina, G. *J. Non-Cryst. Solids* **2001**, *25*, 293.
(6) Cannas, C.; Casula, M. F.; Concas, G.; Corrias, A.; Gatteschi, D.; Falqui, A.; Musinu, A.; Sangregorio, C.; Spano, G. *J. Mater Chem.* **2001**, *11*, 3180.
(7) Komarneni, S. *J. Mater. Chem.* **1992**, *2*, 1219.
(8) Newnham, R. E.; McKinstry S. E.; Ikaua, H. *Mater. Res. Soc. Symp. Proc.* **1990**, *175*, 161.
(9) Ennas, G.; Casula, M. F.; Falqui, A.; Gatteschi, D.; Marongiu, G.; Piccaluga, G.; Sangregorio, C.; Pinna, G. *J. Non-Cryst. Solids* **2001**, *1*, 293.
(10) Casula, M. F.; Corrias, A.; Paschina, G. *J. Mater. Chem.* **2002**, *12*, 1505.
(11) Casula, M. F.; Corrias, A.; Falqui, A.; Serin, V.; Gatteschi, D.; Sangregorio, C.; de Julián Fernández, C.; Battaglin, G. *Chem. Mater.* **2003**, *15*, 2201.
(12) MacLaren, J. M.; Schulthness, T. C.; Butler, B. H.; Sutton, R.; McHenry, M. *J. Appl. Phys.* **1999**, *85*, 4833.
(13) Nagaraju, N.; Fonseca, A.; Konya, Z.; Nagy, J. B. *J. Mol. Catal. A: Chem.* **2002**, *181*, 57.
(14) Corrias, A.; Casula, M. F.; Ennas, G.; Marras, S.; Navarra, G.; Mountjoy, G. *J. Phys. Chem. B* **2003**, *107*, 3030.

10.1021/cm049796h CCC: $27.50
Published on Web 07/09/2004

the intrinsic differences in the growth of the nanoparticles within an aerogel or xerogel SiO_2 matrix, characterized by different porosities and surface coverages.

For this reason, it is very interesting to investigate the possibility of obtaining the FeCo alloy nanoparticles within a different matrix, such as Al_2O_3. The matrix is expected to play a significant role not only in the formation and growth of the dispersed nanoparticles but also on the resulting magnetic properties of the nanocomposite aerogels.

In this work, FeCo−Al_2O_3 nanocomposite aerogels were studied together with pure alumina aerogels which were prepared as a reference material. The alumina aerogel is in itself of interest since this system has not been studied in as much detail as silica aerogel. The samples submitted to thermal treatments both in oxidizing and reducing conditions were characterized by thermogravimetric analysis (TG), differential thermal analysis (DTA), N_2 physisorption at 77 K, X-ray diffraction (XRD), transmission electron microscopy (TEM), and extended X-ray absorption fine structure (EXAFS) spectroscopy. Measurements of magnetization as a function of temperature were performed on the reduced samples by a superconducting quantum interference device (SQUID) magnetometer.

2. Experimental Section

A fast sol−gel synthesis similar to the one described in ref 15 was adopted to prepare the Al_2O_3 alcogel: aluminum tri-*sec*-butoxide ($Al(OC_4H_9^{sec})_3$, Aldrich 97%, ASB), was dissolved in ethanol (Carlo Erba 99.8%, EtOH) at 80 °C and partially hydrolyzed with water diluted in ethanol containing nitric acid, the pH of this hydrolyzing solution being lower than 1. A clear sol was obtained after stirring for about 2 h at 80 °C, and then a final amount of water diluted in ethanol was added after cooling to room temperature. A transparent and clear alcogel was obtained after about 2 h (the Al/H_2O/EtOH molar ratios were 1/1.6/63 and the Al/HNO_3 molar ratio was 1/24). The procedure was slightly modified for the preparation of the FeCo−Al_2O_3 gels. In this case a solution of metal nitrates ($Fe(NO_3)_3 \cdot 9H_2O$, Aldrich, 98%, and $Co(NO_3)_2 \cdot 6H_2O$, Aldrich, 98%) in ethanol was added in the prehydrolysis step; as a consequence, the water needed for the partial hydrolysis of ASB arises entirely from the nitrates. Moreover, no nitric acid was needed, the nitrates solution having a pH lower than 1 as the solution used in the prehydrolysis step for the Al_2O_3 sample. FeCo−Al_2O_3 transparent alcogels were obtained also in this case about 2 h after adding the final portion of water diluted in ethanol. The total metal amount in the final nanocomposite was 10 wt % (Fe + Co/Fe + Co + Al_2O_3) and the Fe/Co molar ratio was 1/1.

The alcogels were aged from 3 h to 3 days before being submitted to high-temperature supercritical drying in an autoclave (Parr, 300 cm^3) filled with an appropriate amount of ethanol. The autoclave was flushed with N_2 and heated at 5 °C·min^{-1} up to 250 °C and then at 1 °C·min^{-1} up to 300 °C. After supercritical drying, the aerogel samples were powdered and calcined at 450 °C in static air for 1 h in order to eliminate the organics. After the first calcination treatment at 450 °C, the samples were either further calcined at increasing temperature from 600 to 1100 °C or reduced under H_2 flow at temperatures between 600 and 800 °C from 2 to 12 h.

Thermal gravimetric analysis (TG) and simultaneous differential thermal analysis (DTA) were carried out on a Mettler-Toledo TGA/SDTA 851. Thermal analysis data were collected in the 25−1000 °C range, under oxygen flow (heating rate = 10 °C·min^{-1}; flow rate = 50 mL·min^{-1}).

XRD spectra were recorded on a X3000 Seifert diffractometer equipped with a graphite monochromator on the diffracted beam. The scans were collected within the range of 5−90° (2θ) using Cu Kα radiation.

TEM bright field (BF) and dark field (DF) images and selected-area electron diffraction (SAED) patterns were obtained on a JEOL 200CX microscope equipped with a tungsten cathode operating at 200 kV. The samples were dispersed in ethanol and dropped on a holey carbon-coated copper grid.

Textural analysis was carried out on a Sorptomatic 1990 System (Fisons Instruments) by determining the nitrogen adsorption/desorption isotherms at 77 K. Before analysis, the samples were heated to 200 °C at a rate of 1 °C·min^{-1} under vacuum. The specific surface area (S), the total pore volume (V_p), and the pore size distributions were assessed by the Barrett−Emmett−Teller (BET) and the Barrett−Joyner−Halenda (BJH) methods, respectively.[16,17]

EXAFS measurements were performed on station 8.1 at the SRS (Daresbury Laboratory, UK). Data were collected at room temperature in transmission mode at the Fe (7112 eV) and Co (7709 eV) K-edges. bcc-Fe and fcc-Co foils were measured as reference compounds. A double Si(111) monochromator was used; higher order harmonic rejection was achieved by detuning the monochromator so that the transmitted flux was reduced by 50%. Data were analyzed using standard procedures.[14]

Measurements of static magnetizations of the samples were performed on a Quantum Design MPMS SQUID magnetometer, equipped with a superconducting magnet producing fields up to 50 kOe. Zero-field-cooled (ZFC) magnetizations were measured by cooling samples in a zero magnetic field and then by increasing the temperature in an applied field of 25 Oe, while field-cooled (FC) curves were recorded by cooling the samples in the same field of 25 Oe.

3. Results and Discussion

3.1 As-Prepared and Calcined Aerogels. In Figure 1A the TG curves of two Al_2O_3 aerogels obtained by supercritically drying gels aged for 3 h and 3 days, respectively, are reported. The weight loss up to 250 °C, generally related to either the presence of adsorbed water on the surface of the sample or solvent residues, is very limited. These data indicate that the supercritical drying procedure is effective in removing the solvent and that the samples are hydrophobic.[18] A sharp but tiny weight loss is observed at about 250 °C followed by the most significant weight loss, which ends at about 550 °C. The aerogel obtained from the gel aged for 3 h presents a larger weight loss compared with the aerogel obtained from the gel aged for 3 days. The corresponding DTA curves, reported in Figure 1C, show two exothermic peaks associated with the weight loss in the region 250−550 °C, the first being very sharp and the second much broader. The second peak is significantly smaller in the aerogel obtained from the gel aged for 3 days in agreement with the lower weight loss. The exothermic peaks were not present when the DTA was performed under inert gas. Therefore, the weight loss can be mainly ascribed to the combustion of organics which can be present in the aerogels either because of nonhydrolyzed alkoxy groups or as a consequence of the esterification of −OH groups by ethanol during the autoclave

(15) Suh, D. J.; Park, T. J. *Chem. Mater.* **1997**, *9*, 1903.

(16) Rouquerol, F.; Rouquerol, J.; Sing, K. S. W. *Adsorption by Powders and Porous Solids: Principles, Methodology and Applications*; Academic Press: London, 1999.

(17) Brunauer, S.; Emmet, P. H.; Teller, E. *J. Am. Chem. Soc.* **1938**, *60*, 309.

(18) Casu, M.; Casula, M. F.; Corrias, A.; Paschina, G. *J. Non-Cryst. Solids* **2003**, *315*, 97.

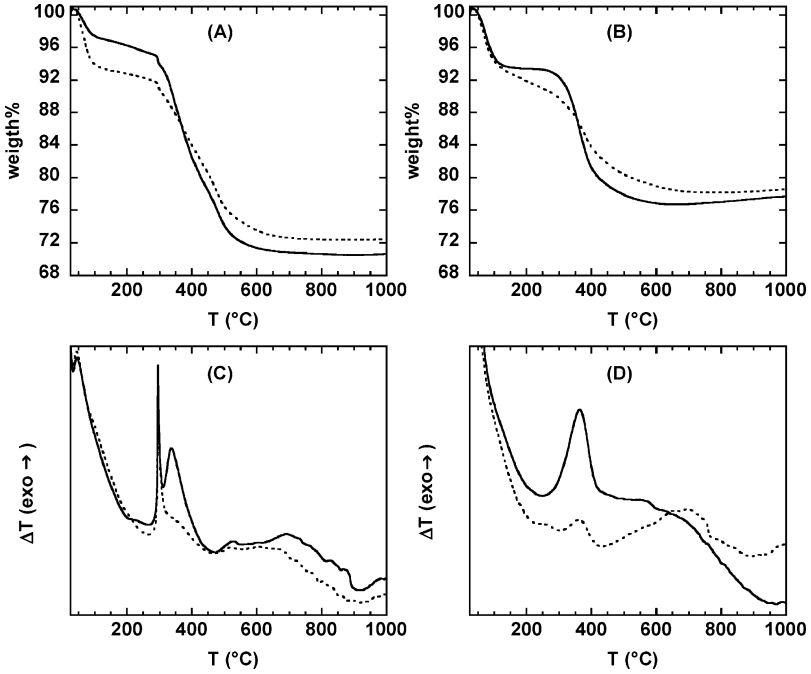

Figure 1. TG curves for the Al_2O_3 (A) and FeCo−Al_2O_3 (B) untreated aerogels obtained from gels aged for 3 h (continuous line) and for 3 days (dotted line) and corresponding DTA curves (C,D).

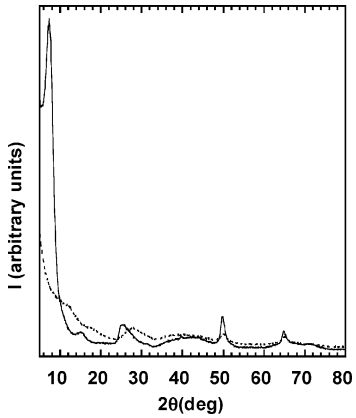

Figure 2. XRD spectra of the Al_2O_3 untreated aerogel (continuous line) and after calcinations at 450 °C (dotted line).

drying process.[18,19] The amount of organics is therefore influenced by the gel aging before supercritical drying.

In Figure 1B the TG curves of two FeCo−Al_2O_3 aerogels obtained by supercritically drying gels aged for 3 h and 3 days are reported. Also in this case the most significant weight loss is observed in the region between 250 and 550 °C and it gives rise to an exothermic peak in the DTA curves, reported in Figure 1D. The weight loss is smaller for the FeCo−Al_2O_3 samples with respect to the Al_2O_3 ones, indicating a lower content of organics; moreover, no sharp weight loss is observed and a single broad DTA peak is observed. As previously observed for the Al_2O_3 aerogels, the aerogel prepared after longer aging presents a lower amount of organics.

The XRD spectrum of the Al_2O_3 aerogel obtained by supercritically drying the gel aged for 3 h, shown in Figure 2, presents peaks corresponding to those of boehmite, AlO(OH), and of the so-called (pseudo)-boehmite. Both phases are characterized by a layered structure in which AlO_6 octahedra are joined by sharing edges forming zigzagged layers, (pseudo)boehmite being actually fine or nanosized boehmite where water molecules adsorbed on the surface lead to a modification of the surface layers.[20] However, the spectrum of the Al_2O_3 aerogel presents an intense peak at about $2\theta = 7°$, which is not ascribed to the boehmite and pseudoboehmite phases. A strong peak at low 2θ is characteristic of the alkyl derivatives of boehmite, named alkoxyalumoxanes, which have the same layered structure of boehmite with pendant alkyl groups between the layers which make the interlayer spacing larger.[21] From the position of the peak at low 2θ, which varies as a function of the alkyl group, the formation of the ethyl derivative can be inferred; this derivative can form as a consequence of the esterification of the −OH groups during the autoclave drying. The formation of the alkoxyalumoxane was confirmed by the presence of several bands due to the stretching and bending modes of alkyl groups in the mid-IR spectra. It is noteworthy that so far the formation of such derivatives has not been reported in Al_2O_3 aerogels preparation. Alkoxyalumoxanes, however, are normally obtained by reaction of either aluminum alkoxide or aluminum metal in primary alcohols at 250−300 °C, conditions close to those of the autoclave supercritical drying. It is also likely that the formation of alkoxyalumoxanes during Al_2O_3 aerogel preparation in an autoclave was not recognized by previous investigations since the characteristic diffraction peak at low 2θ might be missed unless the pertinent range is explored. The present findings confirm that the structure of boehmite can produce sort of intercalation compounds where organic moieties are incorporated between the layers.[21] The spectrum of the Al_2O_3 aerogel

(19) Prassas, M.; Phalippou, J.; Zarzycki, J. *J. Mater. Sci.* **1984**, *19*, 1656.

(20) Tettenhorst, R.; Hofmann, D. A. *Clays Clay Miner.* **1980**, *28*, 373.

(21) Inoue, M.; Kimura, M.; Inui, T. *Chem. Mater.* **2001**, *12*, 55.

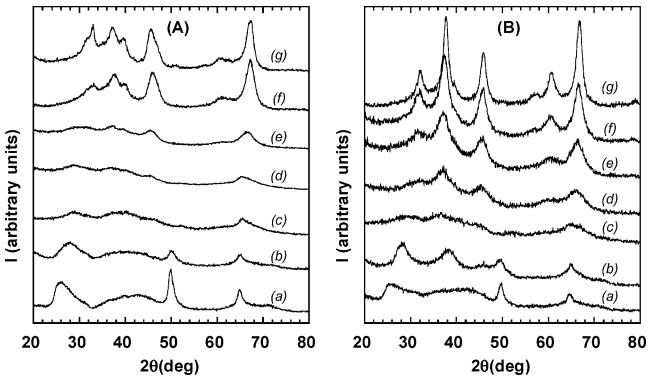

Figure 3. XRD spectra of the Al_2O_3 (A) and FeCo−Al_2O_3 (B) samples. Untreated (a) and calcined at 450 °C (b), 600 °C (c), 700 °C (d), 800 °C (e), 900 °C (f), and 1000 °C (g).

obtained from the gel aged for 3 days (not reported in the figure) is very similar to the one of the sample obtained from the gel aged for 3 h. The only difference is that the peak at $2\theta = 7°$ is slightly smaller in the sample aged for 3 days, indicating that the amount of organic moieties is influenced by the gel aging. After calcination at 450° C the peak at low 2θ disappears together with the mid-IR bands due to the alkyl groups, confirming that the removal of organics is correlated to the disappearance of the ethoxyalumoxane. No difference was observed in the spectra of the two samples obtained from gel aged for 3 h and 3 days after treatment at 450 °C.

In Figure 3A the XRD spectra of the Al_2O_3 aerogel sample and after calcination at increasing temperature are shown in the range from $2\theta = 20°$ to $2\theta = 80°$. Calcination up to 700 °C gives rise to an increasingly disordered phase while at 800 °C new peaks ascribed to the formation of cubic γ-Al_2O_3 begin to appear. At 900 °C peaks due to γ-Al_2O_3 are clearly evident; the presence of a peak at about $2\theta = 33°$ also indicates the presence of a small amount of monoclinic θ-Al_2O_3. At 1000 °C γ-Al_2O_3 is still the predominant phase but θ-Al_2O_3 content increases and finally α-Al_2O_3 begins to crystallize at 1100 °C. The observed structural evolution is in agreement with the phase transformations observed in boehmite-derived gels: metastable γ-Al_2O_3, widely used in catalysis, is formed first and then it evolves toward the thermodynamically stable phase, α-Al_2O_3 (corundum), through polymorphic phase transformations.[22]

In Figure 3B the XRD spectra of the FeCo−Al_2O_3 aerogel calcined at increasing temperature are reported together with that of the untreated aerogel. In this case no peak at low θ was present in the untreated aerogel, indicating that the presence of Fe and Co ions does not allow the formation of an alkyl derivative with the same interlayer spacing as in the Al_2O_3 aerogel. Moreover, the (pseudo)boehmite peaks have a lower intensity compared to the corresponding Al_2O_3 sample, confirming that a more disordered phase is obtained. Calcination to temperatures up to 700 °C gives rise to an increase in disorder while new peaks begin to appear at 800 °C, which are in the same position as γ-Al_2O_3 but have different intensity ratios. This suggests that a phase with a similar structure to γ-Al_2O_3 is obtained where Fe and Co ions partially fill the vacancies. The phase is stable up to 1000 °C while at 1100 °C α-Al_2O_3 and Fe(Co)Al_2O_4 crystallize. These results are significantly different from those obtained for FeCo−SiO_2 aerogels, where calcination led to the formation of metal oxide nanoparticles dispersed in the amorphous silica matrix.[9,10] Such differences can be ascribed to the crystalline structure of γ-Al_2O_3 that can easily accommodate metal ions. In fact, γ-Al_2O_3 has a cation-deficient spinel structure and can easily react with metal oxides.[22] $FeAl_2O_4$ and $CoAl_2O_4$ both have the normal spinel structure with the Al(III) ions in octahedral positions and Fe(II) or Co(II) ions in tetrahedral positions. The evolution of the samples with calcination treatments is also accompanied by a change in color: the aerogels present a greenish color for calcination treatments up to 700 °C while a light blue color characterizes the samples treated at higher temperatures. It should be noted that $CoAl_2O_4$ is characterized by a bright blue color which makes it widely used as an inorganic ceramic pigment.[23]

Figure 4A,B shows the bright field (BF) TEM images of the Al_2O_3 and FeCo−Al_2O_3 calcined at 450 °C, while in Figure 4C−F the BF and corresponding dark field (DF) images of the same samples calcined at 900 °C are reported. The BF images of the samples calcined at 450 °C show the presence of needlelike aggregates; the corresponding DF images (not reported here) indicate that the needles are constituted of chains of round nanocrystals (diameter less than 5 nm). This texture was previously observed in alumina gels and associated with boehmite structure.[22] The BF and DF images of both samples calcined at 900 °C indicate that their texture presents aggregates of round particles with larger average size in FeCo−Al_2O_3 compared to those of the Al_2O_3 sample. Moreover, the particle size distribution is narrow in the Al_2O_3 sample while some significantly larger particles are present in FeCo−Al_2O_3. This difference between Al_2O_3 and FeCo−Al_2O_3 calcined at 900 °C is then ascribed to the presence of particles likely containing Fe, Co, and Al in agreement with the electron SAED (not shown) and XRD patterns.

TEM observations show the presence of a porous texture both in pure alumina and in the composite samples. The presence of an extended porosity is also suggested by the low density of the untreated parent aerogels, around 0.03 g·cm^{-3} for both Al_2O_3 and FeCo−Al_2O_3 samples.

The porous structure of the samples was further investigated by N_2 physisorption measurements. Figure 5A,C,E shows the physisorption isotherm and the corresponding calculated pore size distribution plot (see inset) of the Al_2O_3 untreated aerogel and of the samples calcined at 450 and 900 °C, respectively. All the isotherms can be classified as type IV and show a limited N_2 uptake at low relative pressure, indicating the presence of a mesoporous structure. The shape of the hysteresis and the pore size distributions, however, point out either the presence of mesopores close to the micropore range or of some slitlike pores in the as-prepared aerogel, and to a lower extent in the sample after calcination at 450 °C. The sample calcined at

(22) Reference 3, pp 600−607.

(23) Bolt, P. H.; Habraken, F. H. P. M.; Geus, J. W. *J. Solid State Chem.* **1998**, *135*, 59.

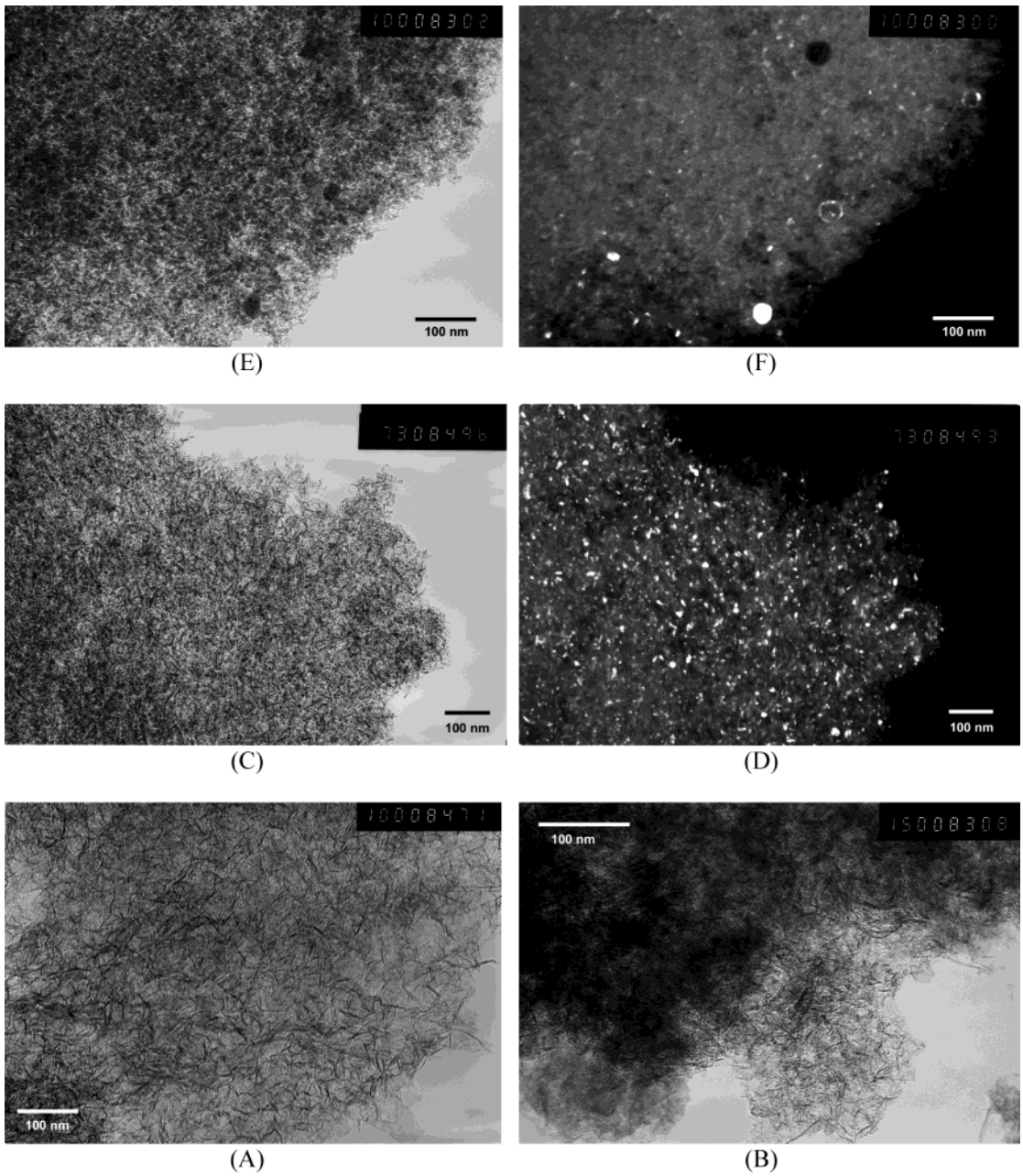

Figure 4. TEM BF images of Al_2O_3 (A) and FeCo−Al_2O_3 (B) calcined at 450 °C; BF and corresponding DF images of Al_2O_3 (C,D) and FeCo−Al_2O_3 (E,F) calcined at 900 °C.

900 °C, on the other hand, only shows the presence of a type H1 hysteresis which is related to the presence of mesopores with a narrow distribution.

Figure 5B,D,F reports the physisorption isotherm and the corresponding pore size distribution plot (see inset) of the FeCo−Al_2O_3 untreated aerogel and of the samples calcined at 450 and 900 °C, respectively. All the samples exhibit a type IV isotherm with an H1 hysteresis loop, indicating the presence of the same network structure.

Table 1 reports the surface area and the pore volume values for the Al_2O_3 and FeCo−Al_2O_3 samples. In the alumina samples, the surface area and pore volumes slightly increase with the calcination treatment at 450 °C and then decreases after further calcinations up to 900 °C. The surface area of the aerogel calcined at 900 °C, however, is still quite large compared with those of γ-Al_2O_3 samples obtained using different methods.[25−27] The surface area values and the pore volumes of the composite aerogels are quite similar to those of the Al_2O_3 samples. In this case the surface area values decrease monotonically with calcinations.

Table 1. Surface Areas (S) and Pore Volumes (V_p) of the Al_2O_3 and FeCo−Al_2O_3 Samples as-Prepared and Calcined at Different Temperatures[a]

	Al_2O_3			FeCo−Al_2O_3		
	as-prepared	450 °C	900 °C	as-prepared	450 °C	900 °C
S ($m^2 \cdot g^{-1}$)	475.25	525.67	228.82	564.22	381.07	223.14
V_p ($cm^3 \cdot g^{-1}$)	1.57	2.08	1.40	3.22	1.74	1.13

[a] Differences in surface area values obtained from repeated runs were found to be less than 5%.

(24) Zayat, M.; Levy, D. *Chem. Mater.* **2000**, *12*, 2763.
(25) Mentasty, L. R.; Gorriz, O. F.; Cadus, L. E. *Ind. Eng. Chem. Res.* **1999**, *38*, 396.

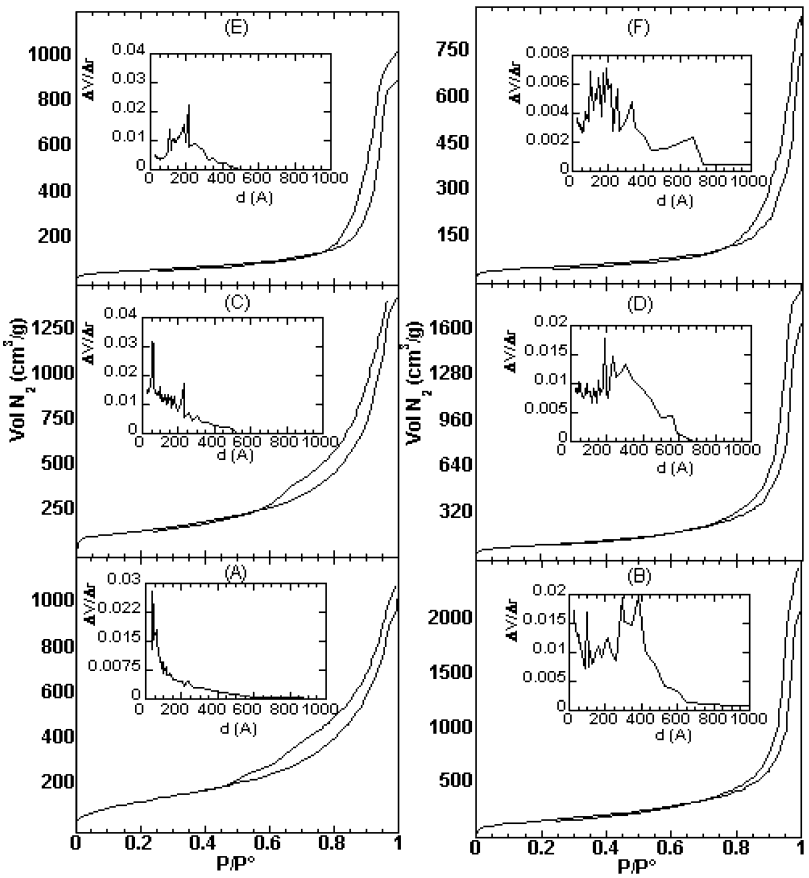

Figure 5. N_2-physisorption curves recorded at 77 K and corresponding calculated pore size distribution (inset) for the Al_2O_3 and FeCo−Al_2O_3 as-prepared aerogels (A,B) and corresponding samples calcined at 450 °C (C,D) and 900 °C (E,F).

The textural characterization indicates that although the as-prepared alumina aerogel is mainly mesoporous, a contribution arising from intraparticle porosity of the layered structure of the ethoxyalumoxane is also present. Combustion of the ethoxy groups at 450 °C results in an increase of the surface area and a reduction of the intraparticle contribution, and finally calcination at higher temperatures leads to uniform mesopores and to a decrease in the surface area. On the other hand, the composite samples present a mesoporous texture which remains almost unaltered upon calcination.

3.2. Reduced Aerogels. In Figure 6 the XRD spectra of the FeCo−Al_2O_3 sample submitted to different reduction treatments in H_2 flow are reported. The spectrum of the sample reduced at 600 °C for 12 h is extremely similar to the one of the same sample calcined at the same temperature and does not show any peak ascribable to the formation of the bcc FeCo alloy; this indicates that the reduction is not effective at this temperature even if the treatment is extended for a long time. On the other hand, after a reduction treatment at 700 °C for 2 h a weak and broad peak at $2\theta = 44.8°$ appears superimposed to those of γ-Al_2O_3, which can be due to the formation of bcc FeCo alloy. It should be pointed out that at the same position a peak due to the matrix is also present, which makes difficult the isolation of the peak due to the alloy; however, the comparison with

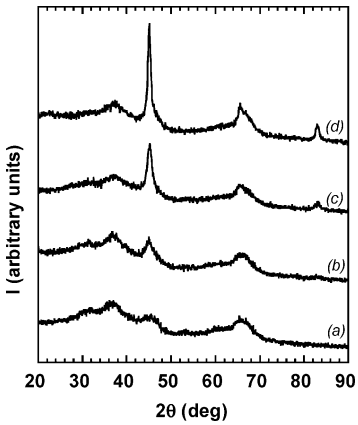

Figure 6. XRD spectra of the FeCo−Al_2O_3 samples reduced at 600 °C for 12 h (a), 700 °C for 2 h (b), 700 °C for 12 h (c), and 800 °C for 2 h (d).

the spectrum of the sample reduced at 600 °C clearly indicates the growth of a new phase. When the reduction at 700 °C is protracted up to 12 h, the intensity of the peak at 44.8° increases significantly and another peak at 82.7° appears, which can also be ascribed to bcc FeCo; these two peaks are even more prominent in the sample reduced at 800 °C for 2 h. It should be pointed out that the XRD cannot give a definite answer on the actual formation of the bcc FeCo alloy, which is difficult to be distinguished from pure bcc α-Fe, the lattice parameter of the two phases being very similar. More detailed information was obtained by taking advantage of the selectivity of the EXAFS technique, which allows one to study separately the Fe and Co environments. The

(26) Grzybowska, B.; Sloczynski, J.; Grabowski, R.; Keromnes, L.; Wcislo, K.; Bobinska, T. *Appl. Catal. A* **2001**, *209*, 279.
(27) Cherian, M.; Someswara Rao, M.; Hirt, A. M.; Wachs, I. E.; Deo, G. *J. Catal.* **2002**, *211*, 482.

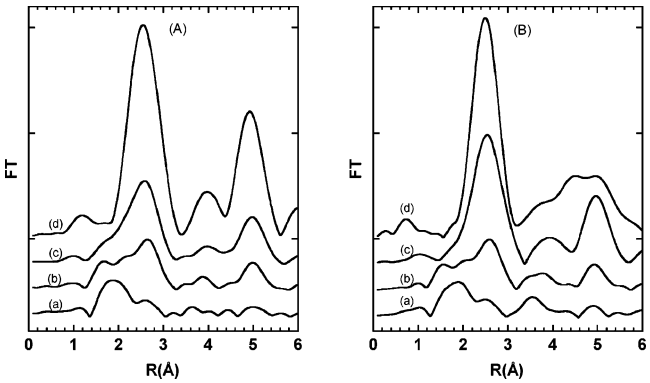

Figure 7. Fourier transforms (phase-shift-corrected) at the (A) Fe K-edge and (B) Co K-edge for the FeCo−Al_2O_3 samples reduced at 700 °C for 2 h (a), 700 °C for 12 h (b), 800 °C for 2 h (c), and for the reference metal foils (d).

quantitative analysis of the EXAFS data is still in progress and will be the subject of another paper. However, the qualitative comparison of the EXAFS Fourier transform (FT) at the Fe and Co edge for the samples reduced at 700 and 800 °C, which are reported in parts A and B, respectively, of Figure 7, provide a definite confirmation on the FeCo alloy formation. In particular, the sample reduced at 800 °C for 2 h is dominated by the presence of the bcc FeCo phase since both FTs look very similar to each other and to bcc Fe and significantly different from fcc Co. In the FTs of the sample reduced at 700 °C for 12 h the main contribution is still due to the bcc phase while a large fraction of Fe and Co in oxide phases can be observed in the sample reduced for 2 h at 700 °C. However, the presence of a shoulder centered at about 2.5 Å, which is completely absent in the EXAFS FTs of Fe and Co oxides,[14]

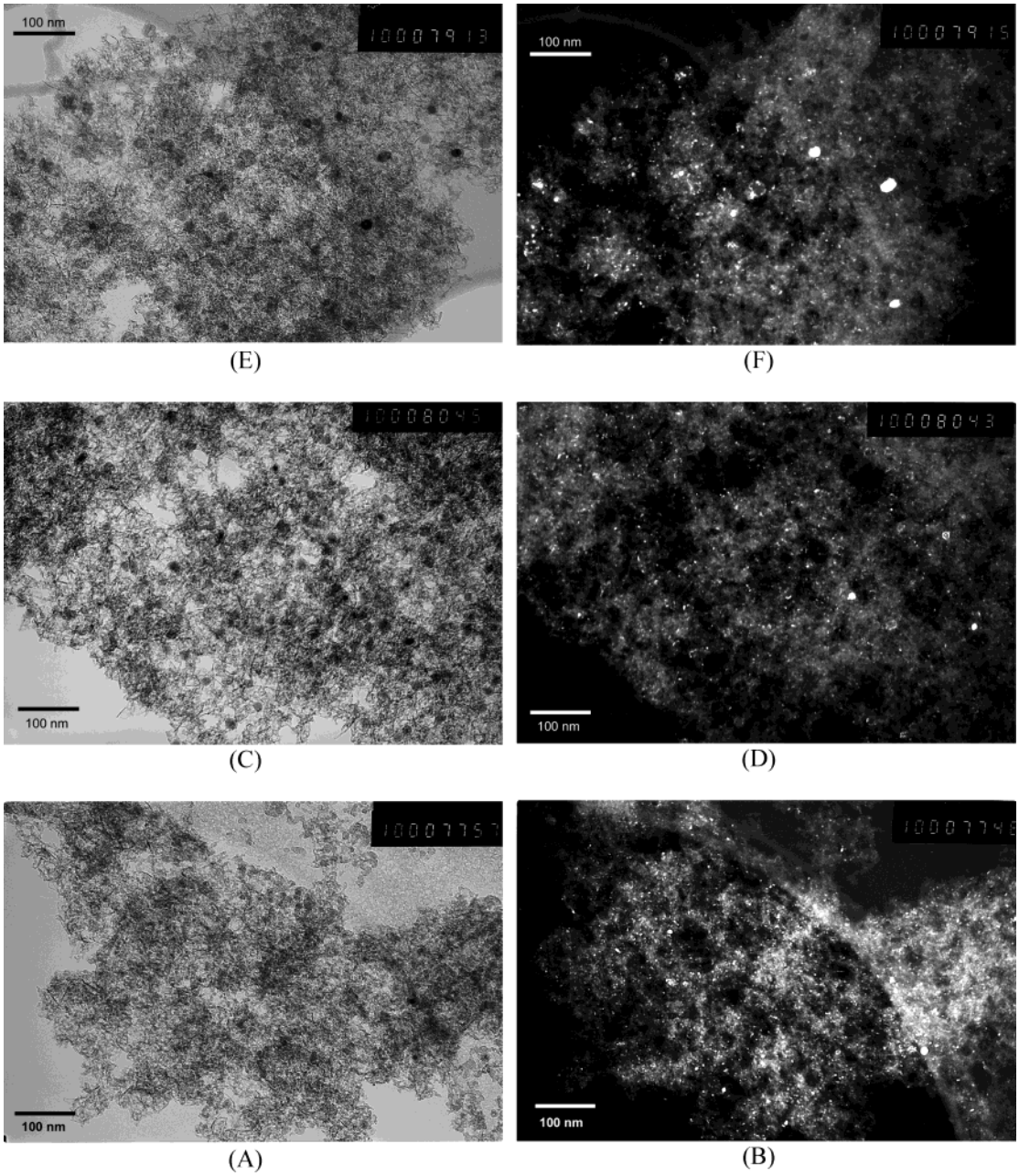

Figure 8. TEM BF and corresponding DF images of the FeCo−Al_2O_3 samples reduced at 700 °C for 2 h (A,B), 700 °C for 12 h (C,D), and 800 °C for 2 h (E,F).

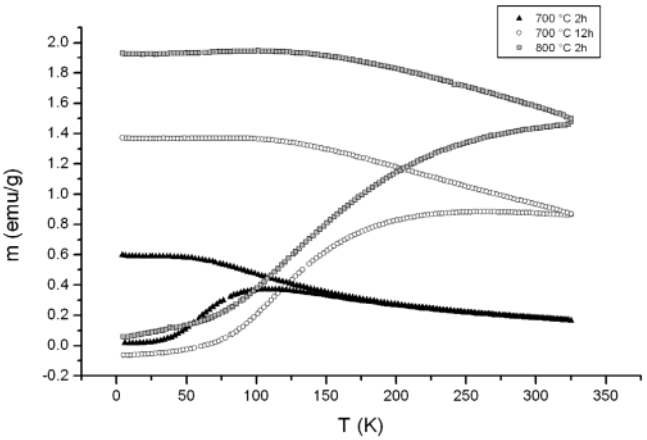

Figure 9. ZFC and FC magnetizations for the FeCo−Al_2O_3 samples reduced at 700 °C for 2 h (▲), 700 °C for 12 h (○), and 800 °C for 2 h (■).

indicates that the metal phase is already formed after this treatment, in agreement with XRD.

In Figure 8A−F the TEM BF and DF images of the FeCo−Al_2O_3 reduced samples at 700 °C for 2 h, at 700 °C for 12 h, and at 800 °C for 2 h are respectively shown. In the BF image of the FeCo−Al_2O_3 sample reduced at 700 °C for 2 h some small round dark spots are detectable, likely due to the FeCo alloy nanoparticles that begin to form, in agreement with XRD results. The texture of the matrix is very similar to the one observed in the samples calcined at 450 °C, with needlelike aggregates constituted by chains of small nanoparticles (<5 nm) as evidenced in the corresponding DF image, where some bigger spots ascribed to the FeCo alloy are also visible. In the samples reduced at 700 °C for 12 h and at 800 °C for 2 h the dark spots are clearly visible in the BF images, the size of the particles being in the range 10−20 nm in the former and larger than 15 nm in the latter sample. The texture of the matrix is the same in all the samples and in all the DF images the small spots due to the nanocrystalline matrix can be differentiated from the bigger spots due to the FeCo alloy.

The FeCo−Al_2O_3 sample obtained by reduction at 800 °C for 2 h is mesoporous, as suggested by the type IV physisorption isotherm with an H1 hysteresis. The sample is still highly porous, having a surface area of 330 $m^2 \cdot g^{-1}$ and pore volumes of 1.60 $cm^3 \cdot g^{-1}$.

Figure 9 reports the ZFC and FC magnetization of the samples reduced at 700 °C for 2 h, at 700 °C for 12 h, and at 800 °C for 2 h, measured in the temperature range of 4.2−325 K. Since it is not straightforward to determine exactly the amount of the FeCo alloy in the samples, because it can vary with time and temperature of the reduction treatment, all the magnetic data are normalized with respect to the entire mass of the sample.

The ZFC and FC magnetizations of the aerogels calcined at 900 °C (not reported here) were also determined and they show pure paramagnetic behavior. On the other hand, in the reduced aerogels superparamagnetic behavior appears as a consequence of the formation and growth of the alloy nanoparticles within the matrix.

In the case of superparamagnetic behavior, at high temperature the ZFC and FC magnetization curves coincide and follow, as a first approximation, a Curie−Weiss law.[28−30] At low temperature the curves begin to separate and the ZFC magnetization exhibits a broad maximum.

It is generally assumed that the temperature of the ZFC maximum, T_{max}, is directly proportional to the average blocking temperature, $T_{max} = \beta T_B$, where β is a constant depending on the shape of the size distribution.[31,32] T_{max}, however, might not be observable in the investigated range. The temperature at which the ZFC and FC curves begin to separate (T_{sep}) corresponds to the blocking of the largest particles. The difference ($T_{sep} - T_{max}$) is therefore a qualitative measure of the width of the energy barrier distribution and thus of the nanoparticle size distribution.

It is noteworthy that the three pairs of ZFC−FC curves reported in Figure 9 present different shapes. In particular, the sample reduced at 700 °C for 2 h shows the typical superparamagnetic behavior: a well-defined maximum, at $T_{max} \cong 100$ K, can be identified in the ZFC curve and above $T_{sep} \cong 260$ K the ZFC and FC magnetizations are completely superposed. This implies that for temperatures higher than 260 K all the nanoparticles are—with respect to the proper measurement's time of static magnetization—in a superparamagnetic state; that is, their magnetic moments can freely oscillate between two opposite directions of easy magnetization.

On the other hand, the ZFC−FC curves of the samples reduced at 700 °C for 12 h and at 800 °C for 2 h are not yet superposing at $T = 325$ K, indicating that these samples contain nanoparticles that at this temperature are still in the magnetic blocked state. Together with the modification of their shape a corresponding increment in the values of magnetization with increasing time and temperature of the thermal treatment is also observed in the three pairs of ZFC−FC curves, which can be mainly ascribed to the formation and growth of the FeCo nanoparticles. In particular, such a trend can be related to the increase of both the mean value and width of the particle diameter distribution pointed out by TEM and XRD measurements, and also of the magnetic interparticle interactions strength.

Preliminary Mössbauer spectroscopy analysis agrees with this picture and also indicates that the alloy retains the equimolar composition in all the samples.[33]

The observation that the FC curve of all the samples is almost constant below a certain temperature suggests the occurrence of interparticle interactions. This behavior can be accordingly ascribed to a transition to a magnetic collective state.[34]

It is not easy to determine the kinds of interparticle magnetic interaction and the way they act on the collective magnetic properties of the investigated samples

(28) Morrish, A. H. *The Physical Principles of Magnetism*; Wiley: New York, 1965.
(29) Nèel, L. *Ann. Geophys.* **1949**, *5*, 99.
(30) Chantrell, R. W.; Wohlfhart E. P. *J. Magn. Magn. Mater.* **1983**, *40*, 1.
(31) Gittleman, J. I.; Abeles, B.; Bozowski, S. *Phys. Rev. B* **1974**, *9*, 3891.
(32) El-Hilo, M.; O'Grady, K.; Chantrell, R. W. *J. Magn. Magn. Mater.* **1992**, *117*, 21.
(33) Concas G. et al., in preparation.
(34) Fiorani, D.; Dormann, J. L.; Cherkaoui, R.; Tronc, E.; Lucari, F.; D'Orazio, F.; Spinu, L.; Nogues, M.; Garcia, A.; Testa, A. M. *J. Magn. Magn. Mater.* **1999**, *143*, 196−197.

but certainly their presence can strongly affect the average magnetic behavior. On the basis of the mean distance between the nanoparticles observed by TEM and the high magnetic moment of FeCo alloy, it is very likely that dipolar magnetic interparticle interactions play the most important role in all the investigated samples. In the case of dipolar interactions their strength increases as the particle magnetic moments (related to particle volume) increase and their distance decreases. Moreover, a partial decrease of the strength of dipolar interactions due to an antiferromagnetic layer on the external surface of the particles cannot be ruled out.

Further studies on the magnetic behavior and in particular on the role of the interparticle magnetic interactions in the investigated samples are still under way and the results will be presented elsewhere.

4. Conclusions

Al_2O_3 and FeCo−Al_2O_3 aerogels with large pore volumes and surface areas were obtained via a fast sol−gel synthesis. The preparation of the pure matrix showed for the first time the formation of the ethyl derivative of boehmite (ethoxyalumoxane) in the processing of alumina aerogels. The ethoxyalumoxane is stable until calcination at 450 °C, which gives rise to a scarcely crystalline compound that upon further calcinations produces nanocrystalline γ-Al_2O_3 stable up to 1000 °C.

Calcination at increasing temperature of the FeCo−Al_2O_3 aerogel gives rise to a phase similar to γ-Al_2O_3 where Fe and Co ions partially fill the vacancies. At the present stage it is not ascertained which is the oxidation state of the metal ions and in which vacancies they preferentially go. This is the subject of an ongoing investigation of the samples using X-ray absorption and Mössbauer spectroscopy techniques.

The reduction of the FeCo−Al_2O_3 samples gives rise to the desired nanocomposites which are constituted of round FeCo alloy nanoparticles embedded into the nanocrystalline γ-Al_2O_3 matrix. It was quite interesting to note that the alloy-Al_2O_3 nanocomposites are obtained even if the calcination of the samples give rise to a single nanophase, as stated above. Therefore, the formation of Fe and Co oxides as intermediate products does not seem to be an essential step. Still, the reduction treatment has to be performed on the samples previously calcined at 450 °C where Fe and Co ions have not gone yet into the γ-Al_2O_3 vacancies; in agreement with this view the reduction of the samples previously calcined at higher temperature does not give rise to the formation of the desired nanocomposites.

The magnetic characterization of the reduced samples indicates that they are superparamagnetic with mean blocking temperature depending on the average size of the FeCo alloy nanoparticles. In particular, the samples treated at 700 °C for 12 h and at 800 °C for 2 h are in a magnetic blocked state still at room temperature.

Acknowledgment. The authors wish to acknowledge Ministero dell'Istruzione, Università e Ricerca (MIUR PRIN), for financial support. The authors thank the European Community-Access of Research Infrastructure action of the Improving Human Potential Program for accessing the SRS Synchrotron.

CM049796H